JTTEE5 18:909–920
DOI: 10.1007/s11666-009-9398-y
1059-9630/$19.00 © ASM International

Numerical Investigation of a Hybrid HVOF-Plasma Spraying Process

B. Martinez, G. Mariaux, A. Vardelle, G. Barykin, and M. Parco

(Submitted February 11, 2009; in revised form August 6, 2009)

This study deals with the numerical investigation of a hybrid thermal spray process that combines HVOF and thermal plasma technologies. In this process, a thermal plasma is used to assist the combustion process that proceeds in a quasi-conventional HVOF system. It is expected that this coupling makes the HVOF system more flexible in terms of working parameters and sprayed materials. Also, a rather low fuel gas consumption and high deposition rate compared to that of most of the conventional HVOF guns are sought. Modeling this process can help to understand the phenomena that control the operation of the spray system and, therefore, help to optimize it. The model involves the plasma formation, combustion process, and expansion of the supersonic jet in the ambient atmosphere. In this study, the system uses argon as plasma-forming gas and methane as fuel gas. Fuel and oxidant are not premixed before entering the combustion chamber. In the model, methane oxidation is represented by a single-step global reaction considering only a few chemical species (fuel, oxidant, and product species); the turbulent non-premixed combustion is modeled by a fast-chemistry combustion model that assumes that the rate of chemical reaction is controlled by turbulence. The model equations are solved using the CFD software Fluent 6.3. The main gas flow characteristics (velocity, temperature, and pressure) in presence and absence of the plasma source are compared and discussed, and the benefits of the plasma source are discussed in the light of predictions and fuel combustion mechanisms.

Keywords Coatings for engine components, HVOF coatings, HVOF process, HVOF spray parameters

1. Introduction

The thermal spray system analyzed in this paper was designed by INASMET Tecnalia and developed in the frame of a European project entitled oxy-fuel ionization (OFI; Ref 1). This new device uses a thermal plasma to assist the combustion process in a HVOF spray torch and, it also uses an auxiliary cold gas to help to control the process temperature.

The point of using an auxiliary cold gas is to make it possible to play on the process temperature. This parameter is particularly important when spraying WC-based powders which are commonly deposited using HVOF, as the in-flight temperature affects the decarburization and solutionizing of the coating hard phases. The control of process temperature by using an auxiliary gas flow was also employed by Katanoda et al. (Ref 2) who added a gas mixing chamber between the combustion chamber and the barrel of a commercial HVOF gun (Praxair-Tafa JP5000). They succeeded to make the gas flow temperature varying between 1,000 and 2,500 K depending on the auxiliary gas flow rate (nitrogen).

The idea of assisting the combustion by thermal plasma is to make the spray system more flexible in terms of working parameters and sprayed materials. It is also expected that this will help to decrease the gas consumption and use fuel with rather low gross heating value, GHV, as natural gas that consists primarily of methane (methane GHV is 39.87 kJ/m^3 compared to 101.25 kJ/m^3 for propane, for instance), even with high powder feeding rate. In the actual OFI system, the latter can be as high as 100 g/min. Finally, it will aid to stabilize the flame over a large range of fuel/oxidant conditions.

The faster the ignition and stable flame are achieved, the more time is available for reaction completion, maximum efficiency, and minimum emissions. The plasma source may bring about a significant decrease in the reaction ignition time that is very sensitive to the mixture equivalence ratio, mixture type, temperature, and pressure. In fact, thermal plasma is supposed to increase the dissociation rate, especially for the initiating step of the chain reactions, to favor multiple branching steps as well it ensures the ignition.

The operation of the OFI torch can be divided in the following consecutive and combined sub-processes (Fig. 1): (i) formation of the thermal plasma jet, (ii) mixing of the plasma jet with an auxiliary cold gas flow, (iii) turbulent combustion, (iv) expansion of the combustion flue gases in the nozzle-barrel and acceleration and heating of the powder particles injected at the barrel inlet, (v) exit of the mixture of combustion flue gases and powder particles into the atmosphere at room conditions

B. Martinez, G. Mariaux, and **A. Vardelle**, Université de Limoges, CNRS, 16 rue Atlantis, 87068 Limoges Cedex, France; and **G. Barykin** and **M. Parco**, INASMET Tecnalia, Polígono Ventas C/Gabiria 8284, 20305 Irun, Spain. Contact e-mail: martinez@ensil. unilim.fr.

Nomenclature

Ar	argon
A	empirical constant, 4.0
a	speed of sound, m/s
B	empirical constant, 0.5
Co	cobalt
C_p	specific heat at constant pressure, J/kg K
C_v	specific heat at constant volume, J/kg K
C_μ	constant of k-ε model, 0.09
$C_{1\varepsilon}$	constant of k-ε model, 1.44
$C_{2\varepsilon}$	constant of k-ε model, 1.92
$C_{3\varepsilon}$	constant of k-ε model, 0
C_{EBU}	empirical constant of EBU model
CH_4	methane
CO_2	carbon dioxide
D_t	turbulent diffusivity, m^2/s
$D_{\alpha m}$	diffusion coefficient of species α in the mixture
D_h	hydraulic diameter, m
E	total specific energy, J/kg
H	hydrogen
H_2O	water
h	specific enthalpy, J/kg
I	arc current intensity, A
I	turbulent intensity, %
J_α	mass diffusion, kg/m^2s
k	turbulent kinetic energy, m^2/s^2
l	Prandtl's mixing length
M	molecular weight, kg/kmol
N_2	nitrogen
O_2	oxygen
Pr_t	Prandtl turbulent number
p	pressure, atm
Q	heat source term, W/m^3
R_i	average rate of production of species ith
R	universal gas constant, kJ/kg K
R	radius, m
Re	Reynolds number
S_p	volumetric generation rate, W/m^3
Sc_t	Schmidt turbulent number
T	temperature, K
U	mean velocity, m/s
u	velocity, m/s
u''	velocity fluctuation, m/s
ν', ν''	stoichiometric coefficients of reactants and products
V	voltage, V
vol	volume, m^3
WC	tungsten carbide
$Y_f''^2$	species fluctuations
Yi	mass fraction of ith species
x	spatial coordinate
p	pressure, Pa
Φ	equivalence ratio
γ	specific heat ratio, C_p/C_v
δ_{ij}	Kronecker delta
ε	turbulent dissipation rate, m^2/s^3
κ	thermal conductivity, W/m K
μ	molecular dynamic viscosity, kg/ms
μ_t	turbulent dynamic viscosity, kg/ms
ρ	density, kg/m^3
σ_ε	constant of k-ε model, 1.3
σ_k	constant of k-ε model, 1
ω	molar reaction rate, mol/m^3s

Subscript

atm	atmospheric conditions
air	air species
EBU	Eddy break up
f	fuel
eff	effective
g	gauge (for pressure)
gas_i	ith gaseous species
inlet_i	ith gas input
i	ith species or derivative index
j	jth species or derivative index
k	turbulent kinetic energy
m	total mass of mixture
max_i	value at the axis
n	normal local coordinate
p	products
r	reactants
t	turbulent
torch	internal torch diameter
α	species
ε	turbulent dissipation rate
τ	tangential local coordinate
∞	room conditions

Superscript

$'$	fluctuation
$''$	variance

Acronyms

CFD	computer fluid dynamics
CPU	central processing unit
EBU	Eddy break-up
EDM	Eddy Dissipation Model
GHV	gross heating value kJ/m^3
HVOF	high velocity oxygen fuel
LTE	local thermal equilibrium
RMS	root mean square
OFI	Oxy-fuel ionization

as an over-expanded supersonic jet, and finally (vi) impact of the sprayed particles onto the part to be covered going with the heating of the part by the gas jet.

Because of the inherent complexity of thermal spray system and difficulty to carry out experiments inside the torch, modeling of such systems is a useful tool to better

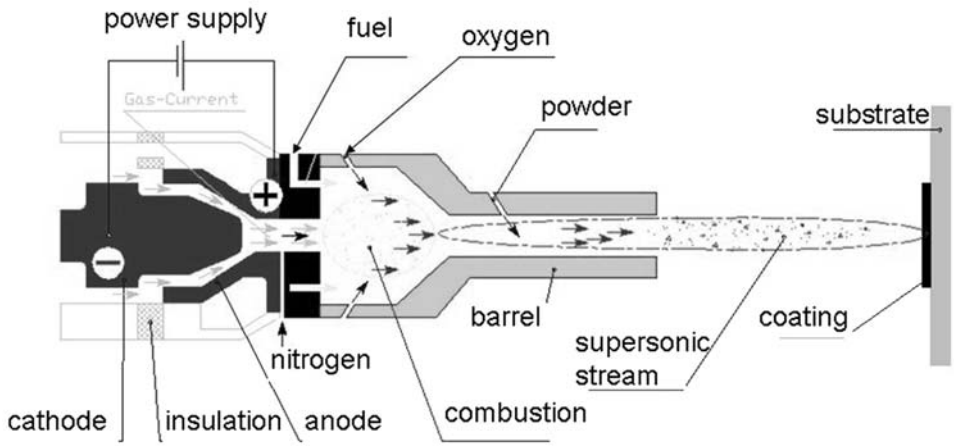

Fig. 1 The OFI spray gun system and its different components

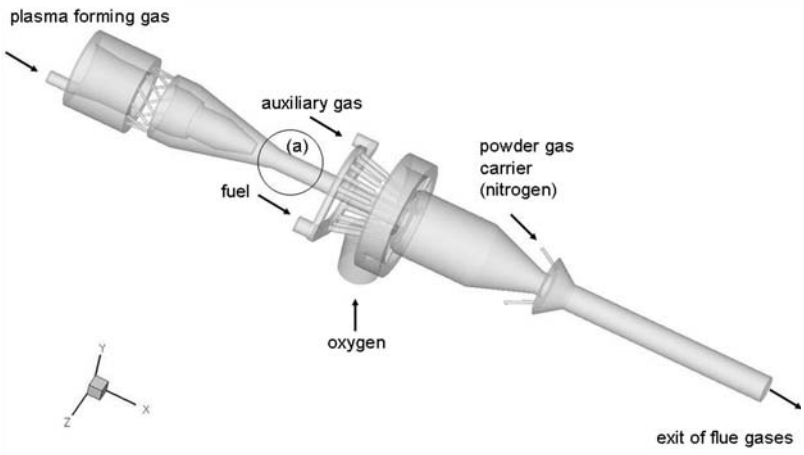

Fig. 2 Three-dimensional internal geometry of the actual OFI gun with the different gas inlets

understand its operation and correlate working parameters and performance.

The objectives of this study, that used computational fluid dynamics (CFD), were to analyze the effect of the plasma and auxiliary gas on the dynamics and temperature of the gas flow inside and outside the OFI system. On account of the involved coupling between the phenomena controlling the process, the methodology was to use a simple model for plasma formation and a well-known and not CPU-expensive model for the combustion process. The common assumption that the chemical reaction rate is much faster than the time-scale associated with the turbulent gas dynamics was used and the phenomenological model of Magnussen and Hjertager (Ref 3) was used. This model called Eddy Dissipation Model (EDM) assumes that reactions occur infinitely fast and reaction rate is limited by the turbulent mixing rate of fuel and oxidant.

In this paper, first, the spray system and its various components are described. The strategy used for the modeling approach and the main steps of the model are then presented. Finally, the predictions of gas flow temperature, velocity, and pressure fields with and without the plasma source are discussed.

2. The OFI Thermal Spray System

The OFI torch is made of three main components: a plasma torch, a combustion chamber, and a barrel of variable length as shown in Fig. 1. The 3D internal geometry of the actual gun is shown in Fig. 2 with the various gas inlets. There are five of them; they correspond to the inlets for the plasma-forming gas, auxiliary gas, fuel gas, oxidant gas, and powder carrier gas. The plasma torch had an internal nozzle diameter of 6 mm; it operated with argon gas at 400 A. This brought about an arc voltage of 30 V and an effective thermal power of 6 kW. Under such conditions, the arc operated in the so-called "*take-over*" mode that corresponds to a diffuse arc attachment on the anode wall and reasonable arc voltage fluctuations (Ref 4-6).

The auxiliary gas (nitrogen) was injected through four injectors located upstream of the combustion chamber.

The fuel gas (methane) and oxidant (oxygen) were not premixed and injected at the entrance of the combustion chamber, via 14 and 6 injectors, respectively. The nozzle-barrel had an internal diameter of 8 mm and a length ranging between 70 and 150 mm. The main operating parameters used in this study are summarized in Table 1. Under these operating conditions, the equivalence ratio Φ was equal to 1.

3. Modeling

3.1 Modeling Strategy and Assumptions

The numerical analysis of the whole system requires the coupling of models for plasma jet formation, gas combustion, and supersonic gas flow expanding outside the torch at room conditions. Preliminary 3D CFD calculations with the geometry shown in Fig. 2 helped to better design the injection of the cold auxiliary gas. Indeed, in the original configuration of the system, this gas whose flow rate can be up to six times higher than that of plasma gas was injected through a single injector and had, thus, a strong tendency to deflect the flow and create an asymmetric plasma jet. Therefore, the injection of cold gas was modified by using four injectors equally distributed along the plasma torch perimeter.

The following sets of computations were carried out with the 2D geometry shown in Fig. 3. It assumed that the system was quasi-symmetrical and includes both the internal and external fields of the gun.

In addition, to simplify the analysis, the conversion from electrical to thermal energy in the plasma gas formation was supposed to occur uniformly throughout a cylindrical portion of the plasma torch. The uniform heat generation was, then, taken into account as a source term in the energy equation.

The combustion process modeling was based on two main assumptions:

(I) The chemical reaction between fuel and oxidant was very fast compared with species transport and so the

Table 1 Main operating parameters of the OFI system used in this study

OFI Gun operating parameters				
	Flow rate			
Gas	slpm	g/s	Gauge pressure, atm	Input temperature, K
Argon	25	0.7	3.94	283
Fuel: CH_4	200	2.2	4.94	283
Nitrogen (carrier gas)	90	1.7	4.94	283
Nitrogen (auxiliary gas)	150	2.9	4.94	283
Oxidant: O_2	400	8.8	9.87	283

Barrel		Electric arc parameters	
Length, mm	Exit ∅, mm	Current intensity, A	Voltage, V
70	8	400	30

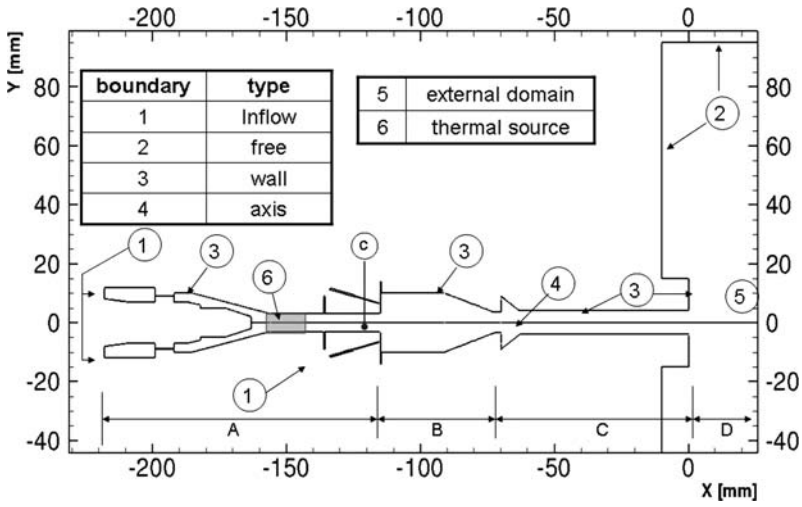

Fig. 3 Two-dimensional calculation domain of the OFI spray system: (A) plasma formation, (B) nonpremixed combustion, (C) powder carrier gas-flame mixing and (D) gas flow expansion. The number notation (1-6) refers the type of boundary conditions used in calculations and the letter notation (c) shows the locations where the predicted profiles shown in Fig. 9 stand

overall rate of reaction was mainly controlled and limited by the turbulent mixing. This assumption is satisfactory for nonpremixed flames as established by the diffusion flame theory (Ref 7, 8), where turbulence convects and mixes fuel and oxidant into the reaction zone. In addition, the temperature increase caused by the plasma jet should lead to an increase in chemical reaction rate but also enhance the dissociation rate of products.

(II) The chemical reaction is represented by a global one-step chemical reaction as follows:

$$CH_4 + O_2 + N_2 + Ar \rightarrow \text{products} \quad \text{(Eq 1)}$$

where the combustion products considered are: CO_2, H_2O, Ar, and N_2.

The reaction represented in Eq 1 supposes that the combustion of CH_4 is complete and that N_2 and Ar species do not participate to the reactions. It also supposes that (i) the combustion products do not dissociate into lower molecular species (OH, H, etc.) as it could be expected at the temperatures reached in the combustion chamber. This global reaction was used for the sake of simplifying the combustion model, even if at stoichiometric conditions, species as CO, OH, NO, O, and H will appear in small quantities. Under stoichiometric and adiabatic conditions and considering these minor species, the temperature reached at the end of an equilibrium combustion process at atmospheric pressure where the reactants are at 300 K is in average equal to 2,230 K (Ref 7, 8). So, assuming no product dissociation and not taking into account the minor species would bring about an overestimate of the predicted gas temperature.

3.2 Gas Flow

The fluid dynamics equations were solved, in the whole computational domain, under the following assumptions: the flow was considered as steady, two-dimensional, dilatable, and compressible. The gas mixture was assumed to be in local thermal equilibrium and optically thin.

The conservation equations consisted of the momentum and energy equations for a multi-species compressible gas mixture, continuity equation for each component of the mixture, and the state relation of ideal gas (Ref 9). They are given in their averaged form after applying *Reynolds* decomposition and the density-weighted *Favre* averaging (Ref 10). Using the *Boussinesq* assumption and the *Einstein* summation convention (for the sake of clarity, the Reynolds, and Favre notations were dropped), they are written as given in Eq 2 to 6:

Mass conservation equation

$$\frac{\partial}{\partial x_i}(\rho u_i) = 0 \quad \text{(Eq 2)}$$

where ρ and u_i are the averaged density and velocity, respectively.

Momentum conservation equation

$$\frac{\partial}{\partial x_i}(\rho u_i u_i) = -\frac{\partial p}{\partial x_i} + \frac{\partial}{\partial x_i}\left((\mu + \mu_t)\left[\left(\frac{\partial u_i}{\partial x_j} + \frac{\partial u_j}{\partial x_i}\right) - \frac{2}{3}\left(\frac{\partial u_l}{\partial u_l}\right)\delta_{ij}\right] - \frac{2}{3}\rho k \delta_{ij}\right) \quad \text{(Eq 3)}$$

where p is the averaged pressure; μ and μ_t are the molecular and turbulent dynamic viscosity, respectively. The symbol δ_{ij} is the *Kronecker* delta tensor operator.

Total energy equation

$$\frac{\partial}{\partial x_i}(u_i(\rho E + p)) = \frac{\partial}{\partial x_i}\left[\rho(\kappa + C_p \mu_t / \mathrm{Pr_t})\frac{\partial T}{\partial x_i} + \sum_\alpha h_\alpha J_\alpha + u_i \tau_{ij\mathrm{eff}}\right] + Q \quad \text{(Eq 4)}$$

where $E = h - \frac{p}{\rho} + \frac{u^2}{2}$, h is the specific enthalpy, $\mathrm{Pr_t}$ is the Prandtl turbulent number, κ the thermal conductivity, and J_α is the mass diffusion in turbulent flow of the α species calculated according to the following expression:

$$J_\alpha = \left(\rho D_{\alpha m} + \frac{\mu_t}{\mathrm{Sc_t}}\right)\nabla Y_\alpha \quad \text{(Eq 5)}$$

where $D_{\alpha m}$ is the diffusion coefficient of the species α in the mixture and $\mathrm{Sc_t}$ the Schmidt turbulent number defined as $\mathrm{Sc_t} = \mu_t / \rho D_t$ with D_t the turbulent diffusivity.

In the case of laminar flows, Eq 5 becomes the diffusion Fick's law; the last term between brackets is the viscous dissipation. The Q term includes the heat production or destruction by chemical reactions ($\sum_{\alpha=1,n} \omega_\alpha \Delta h^0_\alpha M_\alpha$, where ω_α is the production/destruction reaction molar rate of the α species, Δh^0_α is its specific formation enthalpy and M_α is its molecular weight) and other volume heat sources like heat released by the electric arc.

Species transport equation

The average mass fraction Y_i of the ith species of the multi-species flow can be written as follows:

$$\frac{\partial}{\partial x_j}(\rho u_j Y_i) = \frac{\partial}{\partial x_j}\left(\left[\rho D_{im} + \frac{\mu_t}{\mathrm{Sc_t}}\right]\frac{\partial Y_i}{\partial x_j}\right) + R_i \quad \text{(Eq 6)}$$

where R_i is the average net rate of production of the species ith by chemical reaction and D_{im} is the diffusion coefficient of this species in the mixture.

3.3 Calculation of Transport and Thermodynamic Gas Properties

The transport and thermodynamic properties of gas mixture were calculated using mixing laws (Ref 11) with temperature-dependent properties for each species, for temperature ranging between 300 and 15,000 K (Ref 12). These properties should also depend on the pressure as the working pressure, in the calculation domain varied between the atmospheric pressure to 6×10^5 Pa. Raffanel showed (Ref 13) that an increase in pressure resulted in a shifting of the peaks of the temperature-variation properties curves toward higher temperatures because of

species ionization and/or dissociation. The average increase was about 5 or 10% for pressures ranging between 10^5 and 8×10^5 Pa. In this study, the thermodynamics and transport properties of gases were calculated at atmospheric pressure except for the density that was subjected to change by one order of magnitude in the calculation domain due to pressure variation. The mixture density was, then, calculated from the temperature-dependent density and mass fraction for each species and a correction factor was introduced to take into account the pressure-variation according to the ideal gas law.

3.4 Turbulence Model

An improved version of the standard k-ε model (Ref 14), called ''k-ε realizable,'' was used in this study. This model is based on a new formulation of turbulent viscosity and a transport equation for the dissipation rate ε derived from an exact equation of the transport of the mean-square vorticity fluctuation. It results in a better representation of the production and dissipation of the kinetic energy, especially in anisotropic turbulent zones and predicts more accurately the spreading rate of round jets. The transport equations for the k-ε realizable model are the following:

$$\frac{\partial}{\partial t}(\rho k) + \frac{\partial}{\partial x_i}(\rho k u_i) = \frac{\partial}{\partial x_j}\left[\left(\mu + \frac{\mu_t}{\sigma_k}\right)\frac{\partial k}{\partial x_j}\right] + G_k - \rho\varepsilon - Y_M \quad \text{(Eq 7)}$$

and

$$\frac{\partial}{\partial t}(\rho \varepsilon) + \frac{\partial}{\partial x_i}(\rho \varepsilon u_i) = \frac{\partial}{\partial x_j}\left[\left(\mu + \frac{\mu_t}{\sigma_\varepsilon}\right)\frac{\partial \varepsilon}{\partial x_j}\right] + \rho C_1 S_\varepsilon - \rho C_2 \frac{\varepsilon^2}{k + \sqrt{\nu\varepsilon}} \quad \text{(Eq 8)}$$

where

$$C_1 = \max\left[0.43, \frac{\eta}{\eta + 5}\right], \quad \eta = S\frac{k}{\varepsilon} \quad S = \sqrt{2S_{ij}S_{ij}}$$

$$G_k = 2\mu_t S_{ij} S_{ji}, \quad \text{with} \quad S_{ij} = \frac{1}{2}\left(\frac{\partial u_j}{\partial u_i} + \frac{\partial u_i}{\partial u_j}\right).$$

The term Y_M is defined by $Y_M = 2\rho\varepsilon M_t^2$, with $M_t = \sqrt{k/a^2}$ where $a \equiv \sqrt{\gamma RT}$ is the speed of sound.

The turbulent viscosity μ_t is computed by combining k and ε as follows: $\mu_t = \rho C_\mu \frac{k^2}{\varepsilon}$

The constants $C_{1\varepsilon}$, $C_{2\varepsilon}$, $C_{3\varepsilon}$, C_μ, and the turbulent Prandtl numbers σ_k and σ_ε for k and ε respectively, have the following default values:

$$C_{1\varepsilon} = 1.44,\ C_{2\varepsilon} = 1.92,\ C_{3\varepsilon} = 0,\ C_\mu = 0.09,\ \sigma_k = 1.0,\ \sigma_\varepsilon = 1.3$$

3.5 Plasma Model

Power generation was assumed to occur uniformly throughout a portion of the plasma torch nozzle. The volumetric generation rate S_p was, then, equal to the instantaneous electric power VI divided by the volume of a cylindrical portion of the nozzle:

$$S_p = \frac{VI}{vol} \quad \text{(Eq 9)}$$

The term S_p was introduced in the source term S_h of the energy equation. The source volume consisted in a cylinder with a radius equal to that of the nozzle and a length equal to 10 mm. This simple model of energy conversion inside the nozzle yielded an acceptable estimation of the plasma flow characteristics provided that the length of the cylinder where the thermal energy is generated and the boundary condition imposed on the anode wall made it possible to meet the actual thermal efficiency of the plasma torch (about 55%).

3.6 Combustion Model

The Eddy-Dissipation Model (EDM) assumes that the chemical reaction is instantaneous but limited by the turbulent mixing rate of fuel and oxidant was used (Ref 15, 16). It is an extension of the Eddy Break Up concept developed by Spalding (Ref 17). The latter model assumes that the net rate of production R_i of the ith species is proportional to the eddy break up frequency, ε/k that is to the averaged species fluctuations of fresh gases $Y_f''^2$ according to the following equation:

$$R = -C_{EBU}\rho\frac{k}{\varepsilon}Y_f''^2 \approx -C_{EBU}\rho\frac{k}{\varepsilon}Y_f(1 - Y_f) \quad \text{(Eq 10)}$$

where C_{EBU} is an empirical constant determined from experimental results. The EDM (Ref 3) proposes a different expression for the net rate of production R_i that depends on the turbulent variables and averaged-mass fraction of reactants Y_r and products Y_p. R_i is given by the smaller (i.e., limiting) value of the reactants (r) and products (p) reaction rate:

$$R_r = \nu_r' M_r A \rho\frac{\varepsilon}{k}\min\left(\frac{Y_r}{\nu_r' M_r}\right) \quad \text{(Eq 11)}$$

and

$$R_p = \nu_p'' M_p A B \rho\frac{\varepsilon}{k}\left(\frac{\sum_p Y_p}{\sum_p^N \nu_p'' M_p}\right) \quad \text{(Eq 12)}$$

where A and B are empirical constants equal to 4.0 and 0.5, respectively, ν' and ν'' are the stoichiometric coefficients of reactants and products of the chemical reaction and M is their molecular weight.

3.7 Boundary Conditions

The main boundary conditions are shown in Fig. 2 and summarized in Table 2. For the different gas inlets, they consisted of imposing the mass flow rate, turbulence intensity, pressure, temperature, and mass fraction of each species (Table 1). At the system free far boundaries, the pressure was set equal to atmospheric pressure; the

Table 2 Boundary conditions

Physical variables	Boundary condition			
	Inlets (Inflow)	Walls		Free boundaries
		Others	Combustion chamber (b)	Axis (a)
Temperature, K	300 (for all gases)	350	450	$T = T'$	$\frac{300}{\partial t_{tan}} = 0$ (c)
Velocity, m/s and mass flow rate, kg/s	$u_{\text{gas}\_j} = \frac{\dot{m}_j}{\rho_j(T)\pi R^2}$	...		$u = u'$	
	$u_{\text{gas}\_j}(r) = u_{\max\_j} \cdot \left(1 - \left(\frac{r}{\text{Rinlet}\_j}\right)^2\right)$				
Pressure, atm	$p = p_g$	$\frac{\partial p}{\partial n} = 0$		$p = p'$	Outgoing flow: $p = p_{\text{atm}}$ else $p + V^2/2 = p_{\text{atm}}$
Mass fraction Y_i for each species $i = CH_4$, O_2, N_2, Ar, and Air	$Y_i = 1$	$\frac{\partial Y_i}{\partial n} = 0$		$Y_i = Y_i'$	Outgoing flow: $\frac{\partial Y_i}{\partial n} = 0$ (c) else $Y_{\text{Air}} = 1$
	$Y_j = 0$ for other gases				
Turbulence variables k (m^2/s^2) and ε (m^2/s^3) by turbulence intensity I (%) and hydraulic diameter D_h	$k = \frac{1}{2}(UI)^2$ and $\varepsilon = C_\mu^{3/2}\frac{k^{3/2}}{l}$ with $I \equiv 0.16(\text{Re}D_h)^{-1/8}$ $l = 0.075R_{\text{torch}}$; $C_\mu = 0.09$	$k = 0$ $\frac{\partial \varepsilon}{\partial n} = 0$ + classical wall logarithmic law		$k = k'$ $\varepsilon = \varepsilon'$	Outgoing flow: $\frac{\partial k_{\text{or}}\varepsilon}{\partial n} = 0$ (c) else $I = 1\%$ and $\frac{\mu_t}{\mu} = 1$

(a) $\Phi = \Phi'$ the symbol Φ' means $d\Phi/dn = 0$ to axis point
(b) The wall temperature is the same when the plasma is switched on or off
(c) τ and n denotes the tangential and normal local coordinates, respectively

turbulent parameters k and ε were computed from the turbulent intensity and turbulent viscosity ratio that was equal to 1. At the wall boundaries, k and ε were computed by a classical wall logarithmic law.

4. Results and Discussion

The results presented in this work deal with:

- the effect of the plasma source on the internal and external gas flow fields,
- a comparison of predictions with some limited experimental data: gas temperature and photography of the shock waves in the supersonic jet.

The combustion model used in these calculations did not make it possible to take into account an increase in the chemical reaction rate that could be brought by the plasma source. Nevertheless, the fluid model allows predicting an increase in gas temperature and expansion as well as gas mixing resulting from the contribution of the plasma source.

Figure 4 shows the static gas temperature flow fields inside and outside the gun when the thermal plasma source was switched on (above) and shut down (below) as well as its axial evolution along the gun axis. In both configurations, the plasma-forming gas (argon) and auxiliary gas (nitrogen) were taken into account in calculations.

When the plasma was on, the gas temperature increased from 300 K up to 13,000 K in the first part of the spray gun, and, then, it decreased when the plasma jet mixed with the N_2 gas just before it entered the combustion chamber. The combustion proceeded at the periphery of the Ar-N_2 jet where fuel mixed with oxidant and gradually spread in the whole domain as the turbulence developed and homogenized the gas flow. As it will be discussed below, the turbulence in the combustion chamber that controlled, to a great extent, the combustion process was strongly affected by the velocity and density differences between the Ar-N_2 jet and gases injected in the chamber. Indeed, the density of these cold gases was about five times that of the hot Ar-N_2 jet.

When the plasma was on, the static temperature on the gun axis was about 2900 and 1495 K at the gun exit and 200 mm downstream, respectively, while it was about 2720 and 1380 K when the plasma was off. The temperature measured at 200 mm downstream by using a K-type thermocouple was about 1270 K when the plasma was on. The difference (15%) between predicted and measured temperature could be explained both by the simplistic reaction scheme represented by Eq 1 and measurement accuracy (thermocouple measurement accuracy was estimated to be 5% under the conditions of the study).

Figure 5-7 shows the variation along the system axis of the gas static pressure, velocity, and Mach number, respectively. In the combustion chamber where the chemical reaction fed energy, the static pressure reached 4 atm when plasma was off and 4.2 atm when it was on.

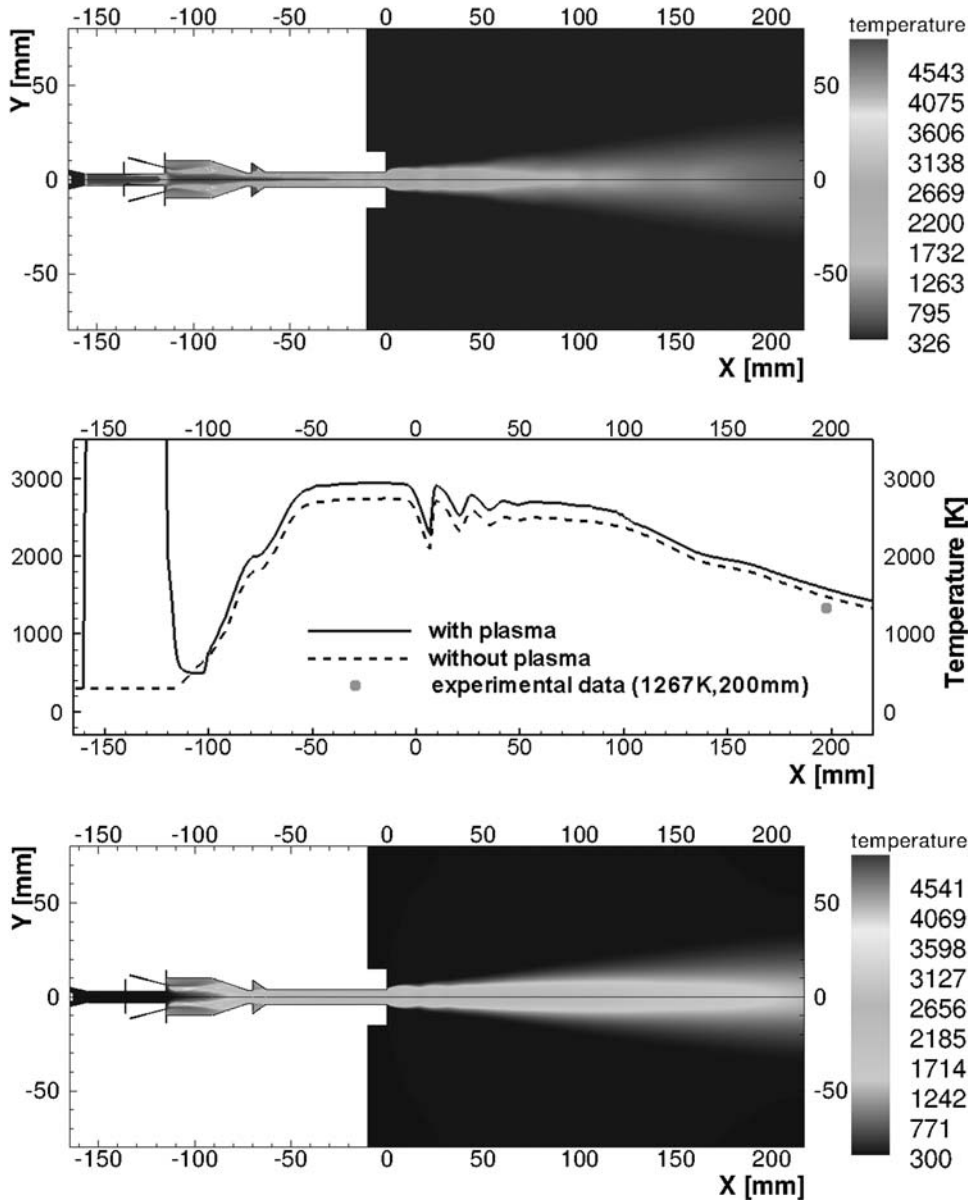

Fig. 4 Static gas temperature (K) flow fields when plasma is on (*above*) or off (*below*) and variation along system axis (*middle*). It should be noted that the color scale is slightly different for the above and below figures

The static pressure, then, decreased down to the ambient pressure at the barrel exit. This decrease proceeded as follows:

- A decrease of 1.75 atm as the gas flow velocity (Fig. 6) increased by 350-400 m/s because of a narrowing of the combustion chamber cross section. When plasma was on the gas velocity was about 350 m/s higher.
- A decrease of about 0.75 atm with an increase in velocity of about 200 m/s as the gas flows expanded in the barrel.
- Finally, a decrease of about 1.5 atm in the free jet. When the plasma was on, the gas velocity was about 250 m/s higher and the shock amplitude was slightly higher. The variation of gas density along the system axis showed that the shock diamonds slightly appeared in the barrel when the plasma was on. This clearly showed that the barrel design needs to be improved to prevent their appearance.

The Mach number remained close to one in the spray gun nozzle and reached 2.4 and 2.6 when plasma was off or on, respectively, in the free jet.

Figure 8 shows a comparison of the predicted velocity (a) and filtered shocks fields (c) with photography of the gas flow outside the spray gun (b). The filtered shocks field for compressible flows showed in Fig. 8c was defined as: $\frac{U}{a} \cdot \frac{\nabla p}{|\nabla p|} = 0$ if $|\nabla p| < 0.1\gamma p_\infty$. It gives an imitated Schlieren

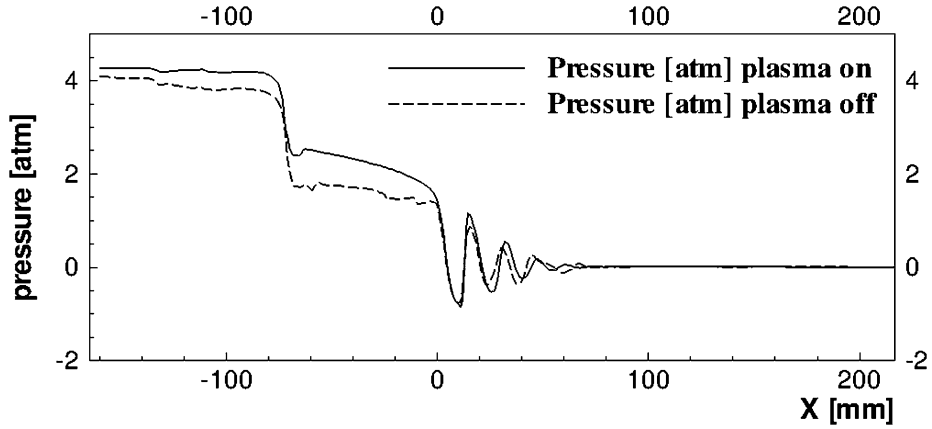

Fig. 5 Static gas pressure (1 atm = 101,325 Pa) along the system axis (the abscissa "0" corresponds to the gun exit)

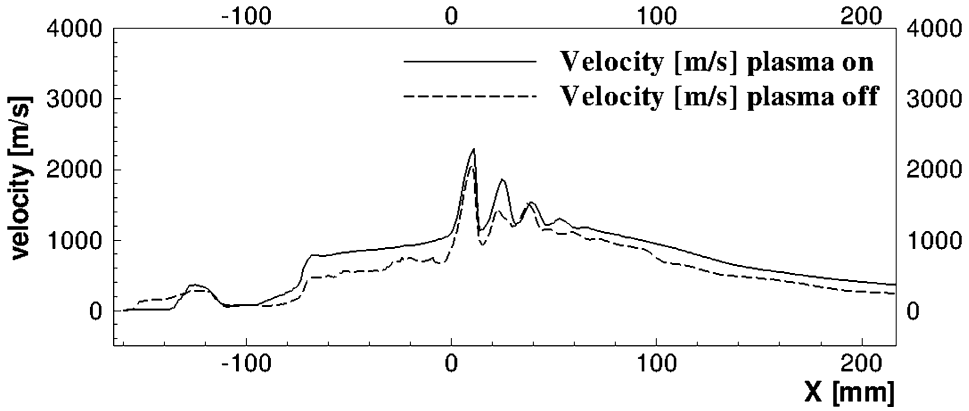

Fig. 6 Gas velocity (m/s) along the system axis (the abscissa "0" corresponds to the gun exit)

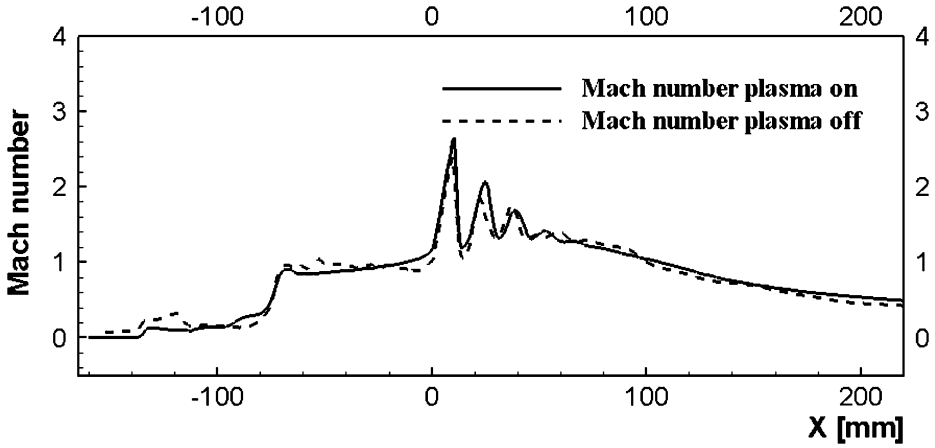

Fig. 7 Mach number values along the system axis (the abscissa "0" corresponds to the gun exit)

visualization for the mean flow field and makes it possible to observe the density variation even if it does not show the value of fluid density The lower section of the figure and photography correspond to the operation of the gun without plasma whereas the upper parts correspond to its operation with plasma. The location of the two-first Mach disks was rather well predicted by the model, but the location of the following disks was slightly shifted. In addition, both made it possible to see the shock diamond near the gun exit.

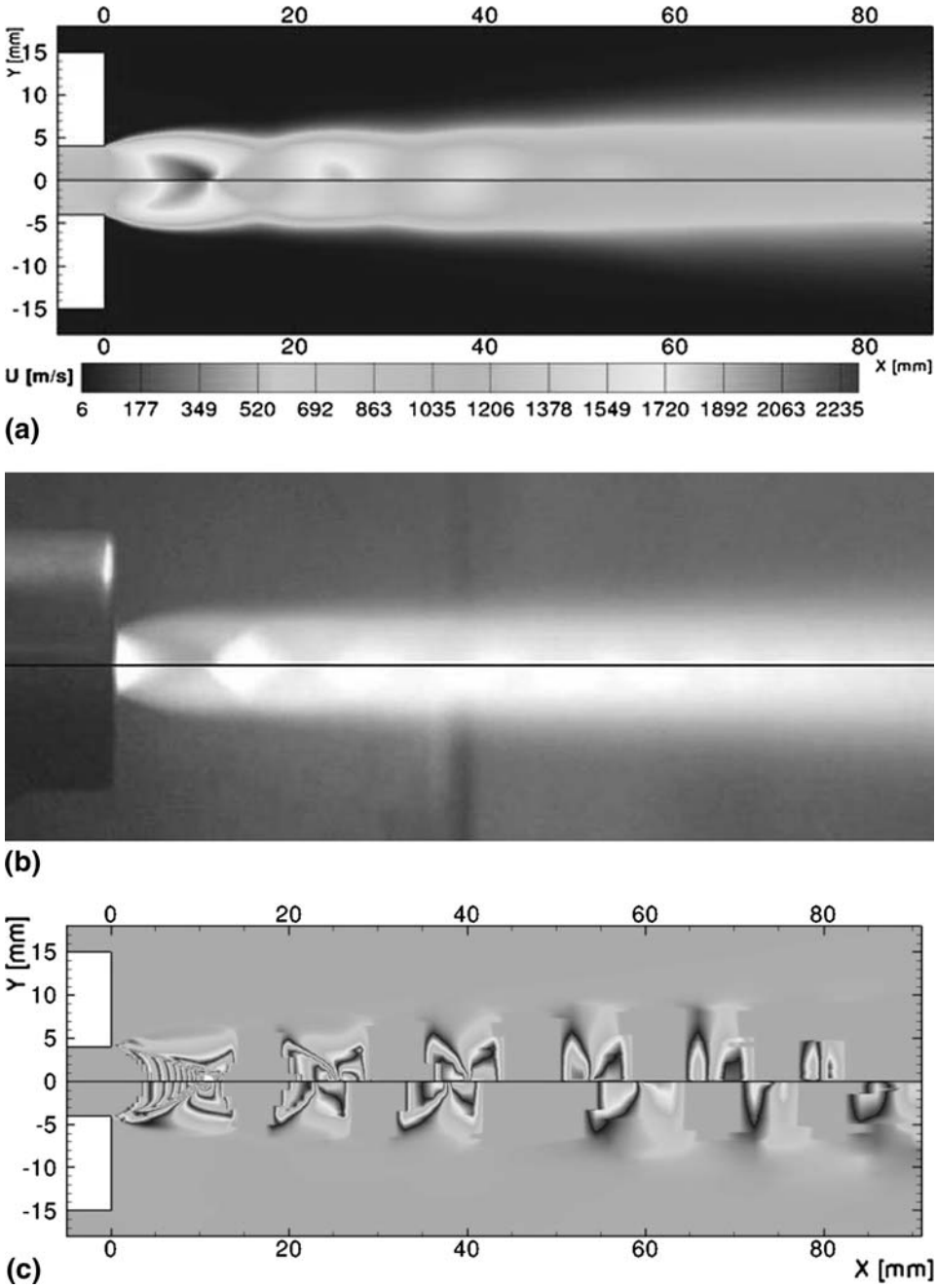

Fig. 8 Comparison of the predicted velocity (a) with jet photographs with plasma (*top*) and without plasma (*below*) (b) and shocks waves field (c)

To sum up, the assistance of the combustion by the plasma jet increased the gas static temperature by about 180 K and lead to a pressure increase by about 0.5 atm in the combustion chamber. It also brought about a rise in gas flow velocity of about 250 m/s and the diamond shocks slightly appeared in the barrel.

As the main objective of this paper was to evaluate and explain the benefits of the plasma source on the combustion process, several assumptions are proposed below to explain the effects observed in the predictions and in the actual system. First, some explanations are given about the particularities of methane gas combustion, especially at temperature greater than 1,500 K.

The oxidation characteristics of methane presents some differences compared to other hydrocarbons due to its large C-H bond energy (40 kJ more than others) and of the produced CH_3 radical that has a lower reactivity compared with alkyl radicals from other hydrocarbons (Ref 18). Therefore, methane combustion requires a high ignition temperature and energy and it results in a low flame speed (Ref 19) due to a large ignition time (about two times this of other fuel) that can be reduced but at

least one order of magnitude (by a factor of 550; Ref 20) by plasma assistance.

The increase in gas temperature helps to break down the hydrocarbon chains into smaller parts like methyl radical CH_3 and favors the apparition of free radicals like OH, O, H, HO_2, CH_3, CHO, etc. that promotes the combustion reactions. In fact, at temperature greater than 1,500 K:

- the classical initiation chain that produces CH_3 by reaction with O_2 for temperature above 800 K, is by-passed by thermal effects.
- multiple chain-branching reactions like $CH_4 + M \rightarrow CH_3 + MH$, $CH_3 + O_2 \rightarrow CH_3O + O$ and $H_2CO + M \rightarrow HCO + MH$ are favored and produce CO relatively fast. Associated to the apparition of OH radical above 1,100 K, they favor the following final oxidation step $CO + OH \rightarrow CO_2 + H$.

Figure 9 that represents the radial variation of the Ar-N_2 gas mixture temperature in a cross section located just before the entrance of the combustion chamber (index "c" in Fig. 3) shows that the plasma source increases the flow static temperature from 300 K to 7,000 K. Therefore, chain initiation and multiple-branching steps should be favored as well as reaction rates.

Nevertheless, these effects are not represented by the one-step chemical model used in this study and a more realistic reaction scheme has to be used in future works.

Also, the thermal energy brought by the plasma contributed to expand the gas that lead to an increase in gas pressure in the combustion chamber; the calculations predicted an increase of about 0.5 atm. Thus, the collisions between chemical species and, so, reactions were slightly favored.

In addition, the plasma jet favored the turbulent mixing of chemical species as the density and velocity differences between the Ar-N_2 jet and the reacting gas injected in the combustion chamber was higher when the plasma source was operating. The predicted radial variation of the turbulent intensity in a cross section located just before the entrance of the combustion chamber inlet showed that the turbulence level of the Ar-N_2 flow reached 50% when the plasma was on as the gas velocity increased from 30 m/s to 200-250 m/s and the density was divided by 20. When the plasma was switched off, the turbulence level of the Ar-N_2 was about 6%.

Figure 10 shows a WC-Co coating manufactured with the OFI system when the plasma source was on (Ref 1). The spraying conditions were that summarized in Table 1 and the powder feed rate was 100 g/min. The morphology of the coating was homogeneous; its averaged hardness was about 1286 HV with a rather low RMS of about 78 HV. As confirmed by the x-ray analysis, the carbide was slightly decarburized during the spray process. However, the values are comparable to those obtained with a Jet Kote gun when using the same powder with a powder feed rate lower than 60 g/min (Ref 21).

5. Concluding Remarks

This paper deals with the study of a new thermal spray process combining HVOF and plasma. A numerical model of the whole system including the plasma source and a simple one-step fast chemistry combustion model were implemented to study the effect of the plasma source on the gas flow fields. The predicted results showed that, in the conditions of the study, the increase in gas

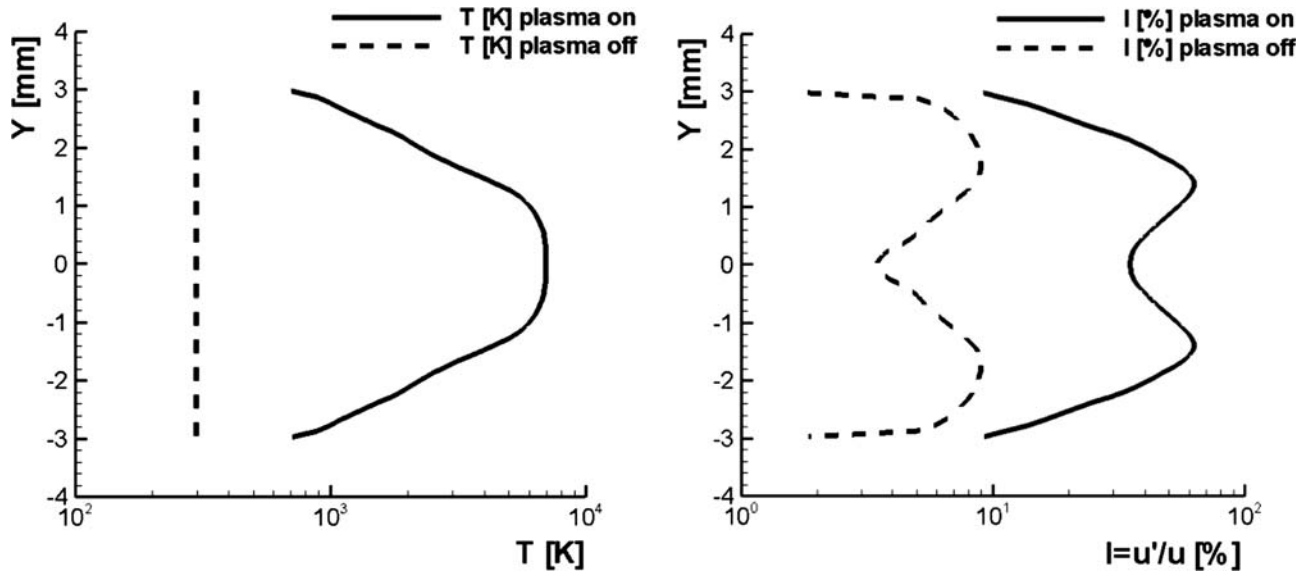

Fig. 9 Radial variation of gas static temperature (K) (*left side*) and turbulent intensity *I* [%] (*right side*), in a cross section located just before the combustion chamber inlet. This cross section is marked by the notation "c" in Fig. 3. It corresponds to a plane orthogonal to gun axis at abscissa −125 mm. *Dashed curve*: "without plasma" and *solid curve*: "with plasma"

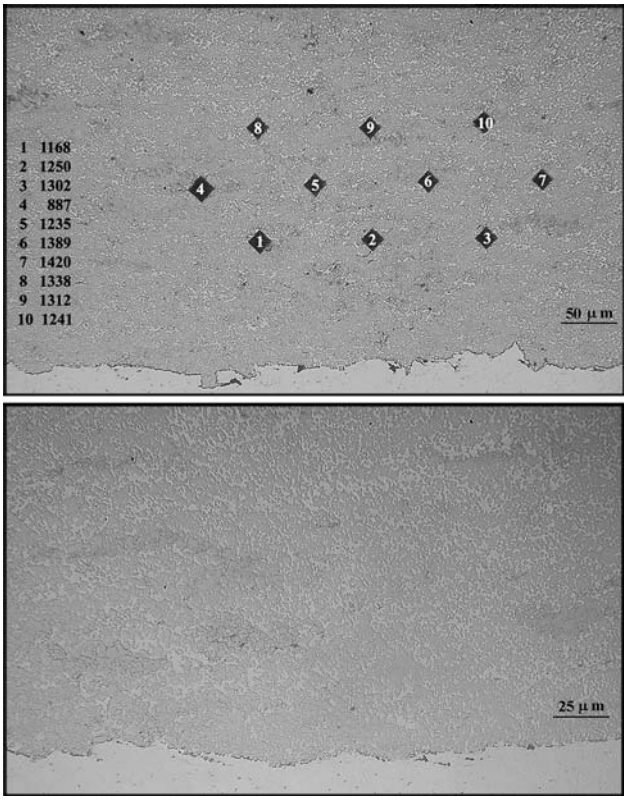

Fig. 10 Cross section of a WC-Co coating manufactured with the OFI system. Powder particle size: 5-45 µm

temperature and velocity when, the plasma was switched on was about 180 K and 250 m/s, respectively. The thermal heating provided by the d.c. plasma jet (6 kW) contributed to the temperature increase and gas expansion as well at the fuel and oxidant mixing due to a higher turbulence level that favored the combustion process. In addition, the temperature increase should bring radicals and ions that favor the combustion rate and its completion.

However, the simplistic reaction scheme and the assumptions used for methane combustion did not make it possible to predict the role of these species. In addition, they also might bring about an overestimate of the combustion temperature. The first step of future work should be to use more developed reaction scheme that takes into account minor species and product dissociation.

At last, WC-Co coating manufactured by using the OFI system with a powder feed rate of 100 g/min showed a homogeneous morphology with a 1254 ± 149 HV.

Acknowledgments

The authors thank the European Community for its financial support through the OFIENGINE project and Dr. B. Pateyron of the University of Limoges, France who kindly supplied the TTwinner software (Ref 10).

References

1. Website: http://ofiengine.com/
2. H. Katanoda, Mathematical Model and Experimental Validation of the Warm Spray (two-stage HVOF) Process. *J. Therm. Spray Technol.*, 2009, **18**(3), p 401–410
3. F. Magnussen and B.H. Hjertager, On Mathematical Models of Turbulent Combustion with Special Emphasis on Soot Formation and Combustion, *Int. 16th Symp. (Int'l.) on Combustion*. The Combustion Institute, 1976
4. M.I. Boulos, P. Fauchais, and E. Pfender, *Thermal Plasmas Fundamentals and Applications*, Plenum Press, New York and London, 1994
5. P. Fauchais, Understanding Plasma Spraying, *J. Phys. D Appl. Phys.*, 2004, **37**, p R86-R108
6. S.A. Wutzke, E. Pfender, and E.R.G. Eckert, Study of Electric Arc Behavior with Superimposed Flow, *AIAA J.*, 1967, **5**, p 707-714
7. S.R. Turns, *An Introduction to the Combustion*, McGraw Hill International Editions, Singapore, 1996
8. R.R. Borghi and M. Champion, *Modeling and Flame Theory*, TECHNIP Editions, France, 2000 (in French)
9. S.B. Pope, *Turbulent Flows*, Cambridge University Press, UK, 2000
10. A. Favre, L.S.G. Kovasznay, R. Dumas, J. Gaviglio, and M. Coantic, *The Turbulence in Fluid Mechanics*, Gauthier-Villars Editors, Paris, France, 1977
11. E.A. Mason and S.C. Saxena, Approximate Formula for the Thermal Conductivity of Gas Mixtures, *Phys. Fluids*, 1958, **1**, p 361-369
12. B. Pateyron, G. Delluc, and N. Calve, T&T Winner, The Chemistry of On-Line Transport Properties in Interval of 300 K to 20.000 K, *Mécanique Industr.*, 2005, **6**(6), p 651-654, website: http://TTwinner.free.fr
13. S. Raffanel, "Thermodynamic and Transport Properties of Nitrogen/Oxygen/Argon Gas Mixtures for $1 < p < 200$ atm and $1000 < T < 30000$ K," PhD thesis, Paul Sabatier University, Toulouse, France, 1987 (in French)
14. T.H. Shih, W.W. Liou, A. Shabbir, Z. Yang, and J. Zhu, A New Eddy Viscosity Model for High Reynolds Number Turbulent Flows Model Development and Validation, *Comput. Fluids*, 1995, **24**(3), p 227-238
15. M. Li and P.D. Christofides, Multi-Scale Modeling and Analysis of an HVOF Thermal Spray Process, *Chem. Eng. Sci.*, 2005, **60**, p 3649-3669
16. M. Li and P.D. Christofides, Computational Study of Particle in Flight Behaviour in the HVOF Thermal Spray Process, *Chem. Eng. Sci.*, 2006, **61**, p 6540-6552
17. D.B. Spalding, Mixing and Chemical Reaction in Steady Confined Turbulent Flames, *Int. 13th Symp. (Int'l.) on Combustion*, The Combustion Institute, 1970
18. J.L. Beduneau, N. Kawahara, T. Nakayama, E. Tomitaa, and Y. Ikedac, Laser-Induced Radical Generation and Evolution to a Self-Sustaining Flame, *Combust. Flame*, 2009, **156**(3), p 642–656
19. S.R. Turns, *An Introduction to Combustion, Concepts and Applications*, McGraw Hill, Ed., ISBN 0-07-114783-7, p 138-143
20. N.L. Aleksandrov, S.V. Kindysheva, I.N. Kosarev, S.M. Starikovskaia, and A.Yu. Starikovskii, Mechanism of ignition by Non-Equilibrium Plasma, *Proc. Combust. Inst.*, 2009, **32**, p 205-212
21. J.G. Legoux et al., Cracking and Spalling Behavior of WC-17% Co Cermet Coatings, *CD-ROM Proceedings of the ITSC*, 2006